# Experimental assessment of emissions maps of a single-cylinder compression ignition engine powered by diesel and palm oil biodiesel-diesel fuel blends

A. Mejía [a], M. Leiva [a], A. Rincón-Montenegro [b], A. Gonzalez-Quiroga [b], J. Duarte-Forero [a,*]

[a] KAI Research Unit, Department of Mechanical Engineering, Universidad del Atlántico, Carrera 30 Número 8–49, Puerto Colombia, Barranquilla, Colombia
[b] UREMA Research Unit, Department of Mechanical Engineering, Universidad del Norte, Barranquilla, Colombia

GRAPHICAL ABSTRACT
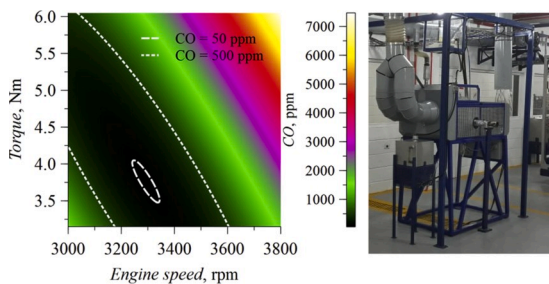
ARTICLE INFO

ABSTRACT

Diesel engines applications cover a broad spectrum, ranging from vehicles that transport passengers and move goods to specialized vehicles and equipment used in the construction and agriculture industries. However, diesel engines are a significant source of pollutant emissions that contribute to poor air quality, negative human health impacts, and climate change. This experimental case study develops emission maps based on statistical models for a single-cylinder, four-stroke, air-cooled diesel engine as a function of torque and engine speed. The tested fuels were 100% diesel (B0), and blends with 5% (B5) and 10% (B10) biodiesel originating from African oil palm (*Elaeis guineensis*). The study explores the individual contributions of NO and NO_2 to NOx and discusses the correlation between CO and O_2 emission maps. The statistical models of CO, CO_2, and O_2 feature R^2 adjusted values greater than 0.8, while the models of NO and NO_2 show R^2

* Corresponding author.
    E-mail address: jorgeduarte@mail.uniatlantico.edu.co (J. Duarte-Forero).

adjusted values of around 0.6. The apparent discrepancies in CO emission trends among previous studies are explained. The emission maps developed here are a practical alternative to predictive models and can assist in engine calibration and aftertreatment optimization while saving time and costs.

Nomenclature

ANN	Artificial neural network
B	Biodiesel content % v/v
BMEP	Brake mean effective pressure
BSFC	Brake specific fuel consumption
BTDC	Before top dead center
BTE	Brake thermal efficiency
Bx	Diesel-biodiesel fuel blends with x volume % of biodiesel
EGR	Exhaust gas recirculation
FAME	Fatty acid methyl ester
H	High level of input variables
HC	Hydrocarbons
L	Low level of input variables
M	Medium level of input variables
MAE	Mean absolute error
N	Engine speed rpm
RSM	Response surface methodology
R^2	Correlation coefficient
T	Torque N·m

---

1. Introduction

Combustion engines are widely used to power road and non-road vehicles as well as small medium-size stationary equipment in several industry sectors [1]. Due to their higher efficiency and durability, diesel engines are preferred over their spark-ignition counterparts for heavy-duty applications and power generation [2]. Although essential to economic growth, diesel engine emissions negatively affect air quality, human health, and global climate. Exhaust aftertreatments such as selective catalytic reduction and particulate filters are typically used to meet the ever-increasing emission standards [3]. The latter have also motivated the development of control and optimization solutions such as exhaust gas recirculation (EGR), high-pressure injection, variable geometry turbochargers, and oxygenated additives [3–5]. This work is focused on the development of emissions maps based on statistical models for a diesel engine powered by diesel and diesel-biodiesel fuel blends. The emissions maps obtained from those statistical models can be used for engine calibration and engine aftertreatment optimization, thus saving time and costs. Those maps are also of great value to assess emissions in stationary operations requiring changes in engine speed, such as in diesel engines coupled to electric alternators or hydraulic pumps.

Humanity faces the challenge of reducing carbon emissions while increasing energy production. Scenarios of the global energy transition to 2040 indicate that the transport sector continues to be dominated by oil, despite increasing penetration of electricity, natural gas, and biofuels [6]. Biodiesel together with diesel-biodiesel and vegetable oil-diesel blends show great potential as alternative fuels for diesel engines [2,7–10]. Biodiesel is an alkyl ester, mostly a fatty acid methyl ester (FAME) in the chain range C_{14}–C_{24}, originating from various renewable feeds such as vegetable oils and animal fats. Biodiesel highly resembles fossil diesel in terms of cetane number, density, and viscosity [2]. A recent literature survey points out that biodiesel and diesel-biodiesel fuel blends influence both performance and emissions of diesel engines [11]. Despite intensive research in the last two decades, published results are still inconsistent in some parameters. Brake specific fuel consumption (BSFC) could increase while brake thermal efficiency (BTE) could either increase or decrease. Carbon monoxide (CO), hydrocarbon (HC), and particulate emissions decrease, but nitrogen oxides (NOx) emissions increase. The carbon dioxide (CO_2) emission could decrease or remain at nearly the same levels of fossil diesel. Oxygen (O_2) concentration increases with a higher content of biodiesel in the blend while smoke opacity reduces.

Predictive models that account for engine processes such as combustion and emissions formation are not the focus here, and the interested reader is referred to Refs. [3,4,12,13]. On the other hand, an artificial neural network (ANN) was capable of accurately predicting the performance and emissions of a diesel engine [14]. Performance and emission maps of a diesel engine were obtained as a function of engine speed and load [15,16]. Likewise, a response surface methodology (RSM) approach was used to study the effect of fuel injection pressure, the start of injection timing, and pilot-main injection intervals on performance and emissions [17]. A method to create engine maps uses data from onboard diagnosis, and portable emissions measurements while vehicles are in actual operation

[18].

Both engine manufacturers and governments are constantly looking for new technologies to reduce emissions and improve fuel efficiency. Only a few studies of engines fueled with diesel and diesel-biodiesel blends cover wide ranges of engine speed and torque. Additionally, there are no detailed studies with a method to construct emissions maps for diesel engines using statistical models. Those emissions maps are an alternative to predictive models and can be used for engine calibration and engine aftertreatment optimization. This case study contributes to closing this gap by combining the design of experiments with the development and validations of statistical models to construct emissions maps. Here we present emissions maps of CO, O_2, CO_2, nitric oxide (NO), and nitrogen dioxide (NO_2). Typically NO and NO_2 emissions are reported together as NOx; as a novelty, here we also explore their individual contribution. Experiments were carried out in a single-cylinder compression ignition engine fueled with diesel and diesel-biodiesel fuel blends covering nine engine operation conditions. The fuels were 100% diesel (B0), and blends with 5% (B5) and 10% (B10) biodiesel content.

2. Materials and methods

2.1. Experimental setup

Fig. 1 shows a schematic diagram of the experimental set-up configuration. The experiments were carried out in a single-cylinder, four-stroke, air-cooled diesel engine (model SK-MDF300, Sokan®). The 3.5 kW generator set-up (SK-GD4000CL, Sokan®) produces alternating current at two voltage levels.

Table 1 summarizes the technical specifications of the engine. The engine has an integrated structure for signal processing through a data acquisition system that acts as an interface between the primary measurement elements and a computer.

Table 2 shows the list of measured variables together with sensor type, accuracy, and measuring range used in this study.

2.2. Exhaust gas analyzer

A portable emissions analyzer (model PCA 400, Bacharach®) was used. The analyzer consists of a sampling probe, an analyzer box, and a control unit, and is equipped with CO, O_2, CO_2, NO, and NO_2 sensors. Table 3 summarizes the technical specifications of the exhaust gas analyzer used in this study.

2.3. Experimental design

The experimental design is composed of different types of variables, namely response, input, blocking, and noise variables. The response variables in the experimental design were gaseous emissions: CO, NO, and NO_2 concentrations in ppm, and O_2 and CO_2 in % v/v. The input variables were torque (N·m), engine speed (rpm), and biodiesel % (v/v) in the fuel. These input variables were chosen due to their influence on engine performance as well as on emissions.
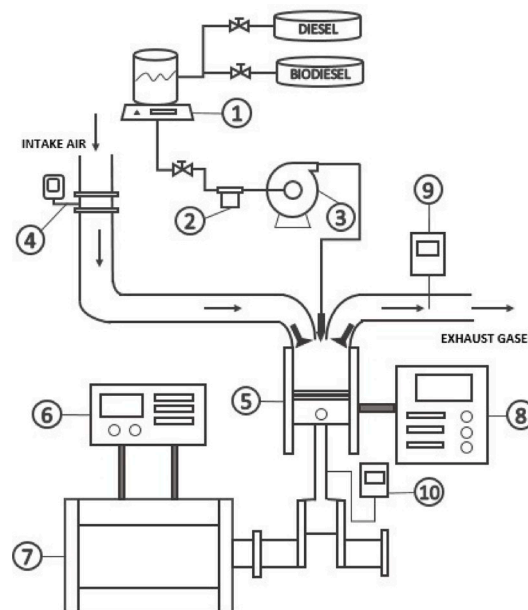

Fig. 1. Schematic diagram of the experimental set-up configuration. Main equipment: ① gravimetric fuel meter, ② fuel filter, ③ injection pump, ④ airflow meter, ⑤ single-cylinder diesel engine, ⑥ resistive test bench, ⑦ alternator, ⑧ data acquisition system, ⑨ exhaust gas analyzer, and ⑩ encoder.

Table 1
Technical specifications of the diesel engine.

Specification	Value/type
Rated power	3.5 kW @ 3600 rpm
Cylinders	1
Strokes	4
Cylinder bore	78 mm
Cylinder stroke	62.57 mm
Displacement	299 cm^3
Compression ratio	20:1
Cooling media	Air
Intake system	Naturally aspirated
Injection system	Direct
Injection Angle	20° BTDC[a]

[a] Before top dead center.

Table 2
Measured variables and sensors specifications.

Variable	Sensor type	Accuracy	Measuring Range
Temperature	Type K thermocouple	0.1%	−200-1370 °C
Pressure	Piezoresistive	0.3%	−100-100 kPa
Fuel mass	Gravimetric meter	2%	0–16 g s^{-1}
Air mass flow rate	Hot wire	1%	0–125 g s^{-1}
Engine speed	Hall effect	0.03%	5–9999 rpm
Relative humidity	Capacitive	2%	0–100%
Atmospheric pressure	Digital barometer	0.5%	30–110 kPa
Electric current	Hall effect	3%	0–100 mA

Table 3
Technical specifications of the exhaust gas analyzer.

Measurement	Range	Accuracy
O_2	0–21% v/v	±0.3%
CO	0–10000 ppm	±10%
NO	0–10000 ppm	±10%
NO_2	0–1000 ppm	±5%
CO_2	0–19.9% v/v	±1%

High (H), medium (M), and low (L) levels were established for each input variable, as can be seen in Fig. 2. At least two levels are necessary to determine the effect of each input variable on the response variables. An intermediate level was included to find out whether the behavior of the response variables within the analysis domain was linear. A multilevel 3^3 experimental design, consisting of the three input variables at three levels, was established. A total of 81 experimental runs were performed, i.e., three results were obtained at each experimental condition. To guarantee the randomness of the experiments, and to minimize unwanted effects caused by uncontrolled ambient factors, the order of the runs was defined with the aid of PSPP (Free Software Foundation, Inc.).
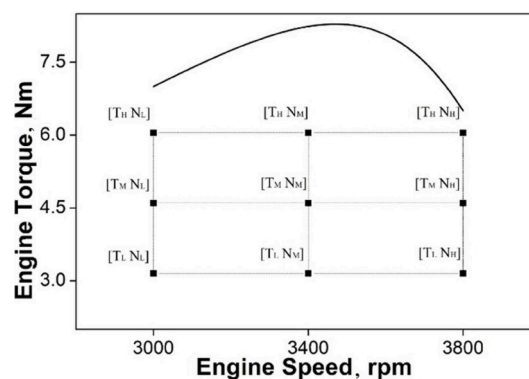
Fig. 2. Operational parameters of the engine used for the experiments. Subscripts H, M, and L refer to the levels of the input variables, T represents torque, and N represents engine speed. The upper curve corresponds to the engine characteristic curve.

The operating modes were chosen, taking into account the most significant points below the engine characteristic curve. In the case of engine speed, the maximum value was 3800 rpm. Since this is the point at which maximum power is reached, working at a lower frequency (e.g., 50 Hz) requires decreasing engine speed. A value of 3000 rpm was taken as the minimum engine speed to cover the range of plausible operating conditions for both stationary and transient applications. For the torque, the selected maximum and minimum values were 6.05 and 3.15 N m, respectively.

Fuel composition is another factor that significantly affects engine emissions. Pure diesel (B0) and diesel-biodiesel blends of 5 and 10% (B5 and B10, respectively) were used. Table 4 summarizes the standardized fuel properties of the diesel and the diesel-biodiesel blends.

Blocking variables are variables that can be quantified, but their influence is not evaluated, such as ambient temperature and fuel temperature. Non-controlled variables are, by definition, difficult to control and could influence the behavior of response variables. Examples of the latter are cylinder head temperature, exhaust temperature, and intake pressure.

This study comprises 81 experimental runs, three at each experimental condition. Data from 80% of the trials were used to fit regression models through variance analysis. Fig. 3 depicts the methodology using the CO emission map for one type of fuel. Fig. 3a shows the raw experimental data, while Fig. 3b shows the emission map obtained from the regression model. Finally, the remaining 20% of the data were used for validation, as illustrated in Fig. 3c.

3. Results and discussion

3.1. Models development

This section describes how statistical models with a significant association between emissions and torque, engine speed, and fuel type were developed. Besides the main effects (torque, engine speed, and fuel type), models also include squared and interaction terms. The p-value for each term was compared to a significance level to determine whether the association between the response and the term was statistically significant. If the p-value was ≤ 0.05, the association between the response and the term was assumed as significant; otherwise, the model was fitted without that term. Table 5 shows the p-values of each of the terms considered for the development of the models.

Models were fitted following either a bottom-up or a top-down terms selection procedure. The bottom-up selection started with a constant to which a term was added at a time. At each step, the algorithm brought into the model the most significant term provided that its p-value was ≤ 0.05. Terms previously brought into the model can be deleted later if their p-values fall below 0.05. The top-down selection started with a model containing all the possible terms. At each step, the algorithm removed the less significant term provided that its p-value was > 0.05. Terms previously deleted can be reentered later if their p-values meet the significance criterion. The resulting top-down and bottom-up models were compared, and the ones with the highest R^2 were selected.

Table 6 summarizes the selected models and their respective R^2, R^2 adjusted, standard error, and mean error absolute. It should be noticed that R^2 represents the percentage of variation in the response that is explained by the model. R^2 adjusted, on the other hand, is R^2 adjusted for the number of predictors in the model relative to the number of observations. The standard error of the estimate represents the standard deviation of the residues, and the mean absolute error is the average of the residues.

3.2. Emissions maps

3.2.1. CO emission map

Fig. 4 shows the CO emission map as a function of engine speed and torque. The CO emission map features three diagonal bands. A central band with relatively low CO emission (≤ 500 ppm) covers the engine speed range 3200–3600 rpm and the torque range 4.2–6.0 N m. An upper band in which CO emission increases significantly (500–7000 ppm) with both engine speed and torque. At those operation conditions, the fuel-to-air ratio gradually increases, and there is not enough time for mixing, which negatively affects combustion quality. A lower band in which CO emission increases (500–2000 ppm) with decreasing both engine speed and torque. At those operation conditions, the lean fuel/air mixture results in relatively low combustion temperatures, which leads to higher CO formation rates.

The emission map in Fig. 4 indicates the presence of a global minimum in CO emission. Minimum values in CO emission are thus found either increasing torque at constant engine speed or increasing engine speed at constant torque. Several studies with fossil diesel

Table 4
Standardized fuels properties of diesel and palm oil biodiesel-diesel blends used in this study.

Property	Standard	B0[a]	B5	B10
Density, kg m^{-3}	ASTM D1298	821.5	823.1	827.5
Viscosity, cSt	ASTM D445	2.64	2.65	2.66
Flash point, °C	ASTM D93	76	85	96
Cloud point, °C	ASTM D2500	6.5	7.2	8.3
Pour point, °C	ASTM D97	3.1	3.5	3.8
High heating value, MJ kg^{-1}	ASTM D240	44.05	43.89	43.25

[a] Pure diesel.

a)   b)
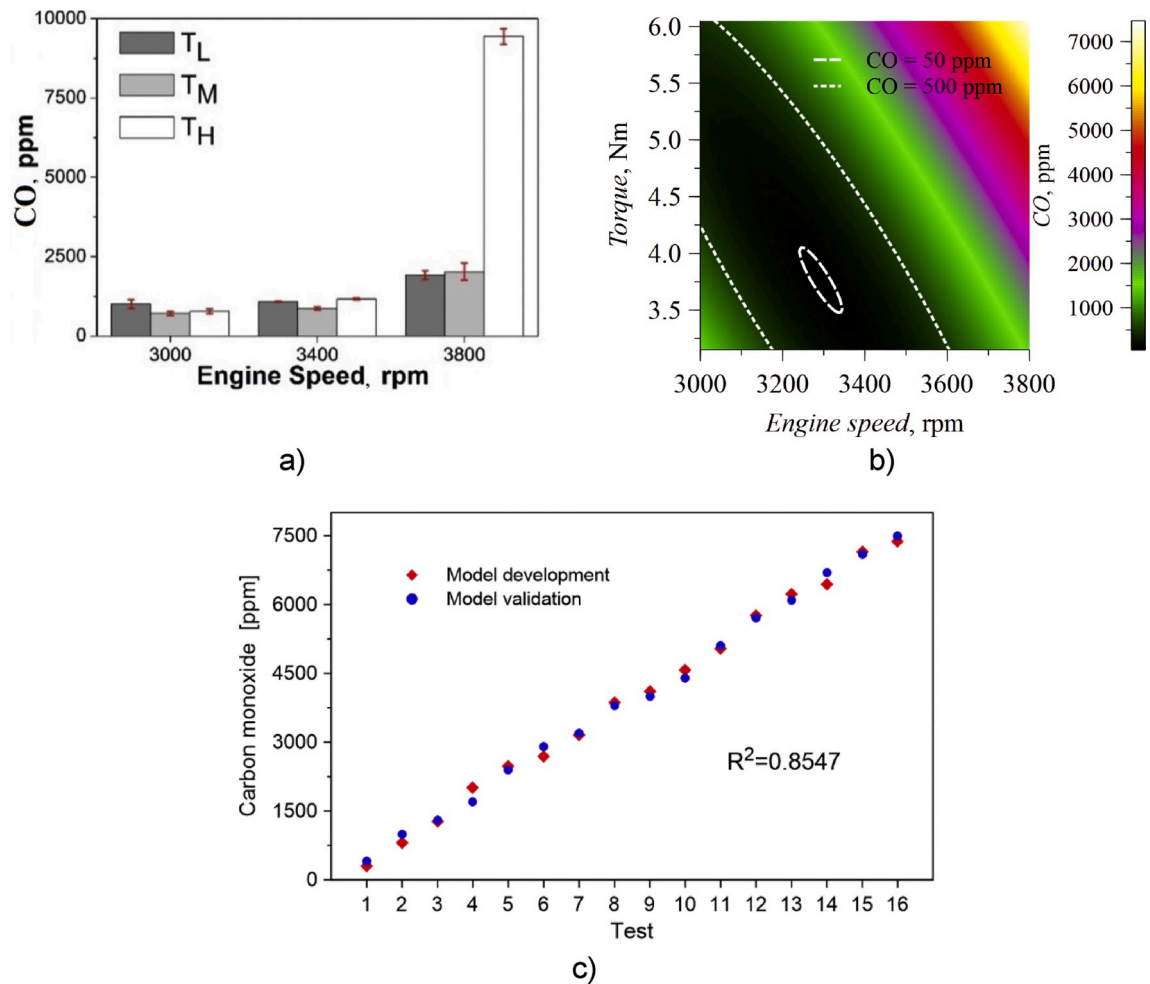

c)

Fig. 3. Methodology used in this study. a) Experimental result for CO emissions for one type of fuel. Error bars represent twice the standard deviation, b) Emissions map predicted by the regression model obtained from the analysis of variance, c) validation of the regression model.

Table 5
P-values as obtained from the analysis of variance.

Factor	CO	CO_2	NO	NO_2	O_2
T:Torque	0.0000	0.0000	0.0000	0.0000	0.0000
N:Speed	0.0000	0.0000	0.9827	0.9961	0.0000
B	0.3983	0.0307	0.0001	0.0001	0.0416
TT	0.0085	0.7926	0.0388	0.0383	0.6179
TN	0.0000	0.0000	0.9198	0.9319	0.0000
TB	0.3322	0.6881	0.0156	0.0156	0.7756
NN	0.0000	0.0070	0.1918	0.0406	0.0000
NB	0.1572	0.4490	0.0001	0.0001	0.0205
BB	0.0589	0.0284	0.5049	0.5201	0.0320

report a minimum in CO emission when torque (also reported as engine load percentage or BMEP) increases at constant engine speed [11,19–23]. Under the same condition, some studies with fossil diesel show either a decreasing [24] or an increasing [25] trend in CO emission. Other studies, in which engine speed increases at full load, show a CO emission increasing trend [26] or a trend with local minima and maxima [27]. The CO emission map in Fig. 4 is consistent with published studies. The apparent discrepancies in trends depend on the location of engine speed and torque ranges with respect to the global minimum.

Our results show that the association between CO emission and fuel type was statistically non-significant. A recent experimental study explored the effect of biodiesel content on CO emissions, increasing engine load at constant engine speed [11]. For engine load in the range 10–80%, there were no significant differences in CO emission for diesel-biodiesel blends lower than B20, which is in

Table 6
Statistical models and selected parameters.

| Model	Model	R^2	R^2 Adj[a]	Standard Error	MAE[b]	Fitting proc[c]
CO	$142445.0021 - 12034.9056 \cdot T - 72.7381 \cdot N + 302.4108 \cdot T^2 + 2.9637 \cdot T \cdot N + 0.0093515 \cdot N^2$	0.8547	0.8455	1027.43	776.494	Asc[d]
CO_2	$35.6719 - 2.1437 \cdot T - 0.02056 \cdot N - 0.1511 \cdot B + 0.0009291 \cdot T \cdot N + 0.000003044 \cdot N^2 + 0.01570 \cdot B^2$	0.8930	0.8760	0.7287	0.4110	Desc[e]
NO	$-166.3510 + 431.9910 \cdot T - 212.5820 \cdot B - 36.9578 \cdot T^2 + 8.9195 \cdot T \cdot B + 0.00004107 \cdot N^2 + 0.05567 \cdot N \cdot B$	0.6455	0.6167	155.29	109.77	Desc
NO_2	$-170.0360 + 455.2360 \cdot T - 225.1740 \cdot B - 39.0805 \cdot T^2 + 9.4100 \cdot T \cdot B - 0.00004374 \cdot N^2 + 0.05900 \cdot N \cdot B$	0.6432	0.6143	163.759	114.94	Desc
O_2	$-47.8265 + 4.0399 \cdot T + 0.03875 \cdot N + 0.6867 \cdot B - 0.001719 \cdot T \cdot N - 0.000005579 \cdot N^2 - 0.0001611 \cdot N \cdot B - 0.01681 \cdot B^2$	0.9533	0.9488	0.8060	0.566781	Des

[a] Adjusted.
[b] MAE: Mean absolute error.
[c] Procedure.
[d] Ascending.
[e] Descending.
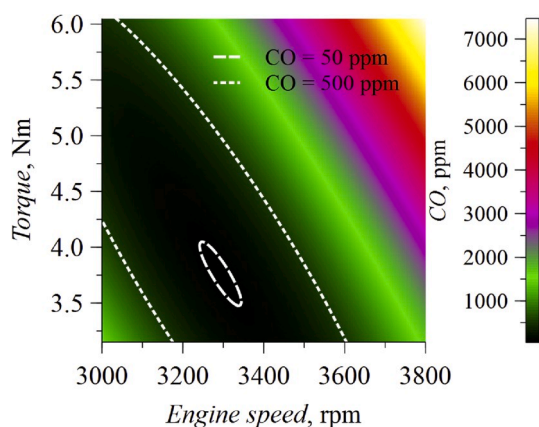
Fig. 4. Emission map of CO. The association between CO emission and fuel type was statistically non-significant. Dashed and dotted lines represent isoconcentration contours.

agreement with our results. Starting from a relatively low engine load, operating with pure biodiesel (B100) results first in a local maximum and then in a local minimum in CO emission. Other studies with pure biodiesel (B100) only report a minimum in CO emission when torque increases at constant engine speed [20,25].

3.2.2. O_2 emission map

Fig. 5a shows the O_2 emission map for the operation with fossil diesel. An inverse proportion characterizes the dependence of O_2 emission on both engine speed and torque. When torque increases by 1.0 N m, O_2 concentration decreases by 1.1% v/v at 3000 rpm and a 2.5% v/v at 3800 rpm. When engine speed increases at constant torque, O_2 emission decreases linearly at first and then more rapidly. The nonlinear dependence of O_2 emission on engine speed is more evident at the higher end of the assessed torque range. The O_2 emission map is consistent with the CO emission map, i.e., the area corresponding to the lower end of the studied engine speed and torque ranges shows the highest O_2 emission and significant CO emission due to relatively low combustion temperatures. Conversely, the area corresponding to the upper end of the studied engine speed and torque ranges shows the lowest O_2 emission due to the relatively high fuel-to-air ratio and lack of mixing.

Studies reporting O_2 emission in the exhaust of diesel engines are rather scarce. A study in which load increases at constant engine speed reports a decreasing O_2 concentration trend [11]. Another study with fossil diesel found that, at constant engine speed, the equivalence ratio increases linearly with BMEP [24]. The O_2 emission map in Fig. 5 is consistent with those findings. Another study, in which engine speed increases at full load, shows a linear O_2 emission trend, as it was expected [26]. On the other hand, a study under similar conditions shows that O_2 emission increases at first, then decreases and finally increases sharply [34]. The latter results, especially those at the higher end of the studied engine speed range, are not evident in our results. This indicates that emissions at full load operation require further attention.

Fig. 5b and c shows the O_2 emission map for the operation with B5 and B10 diesel-biodiesel blends. With respect to the operation
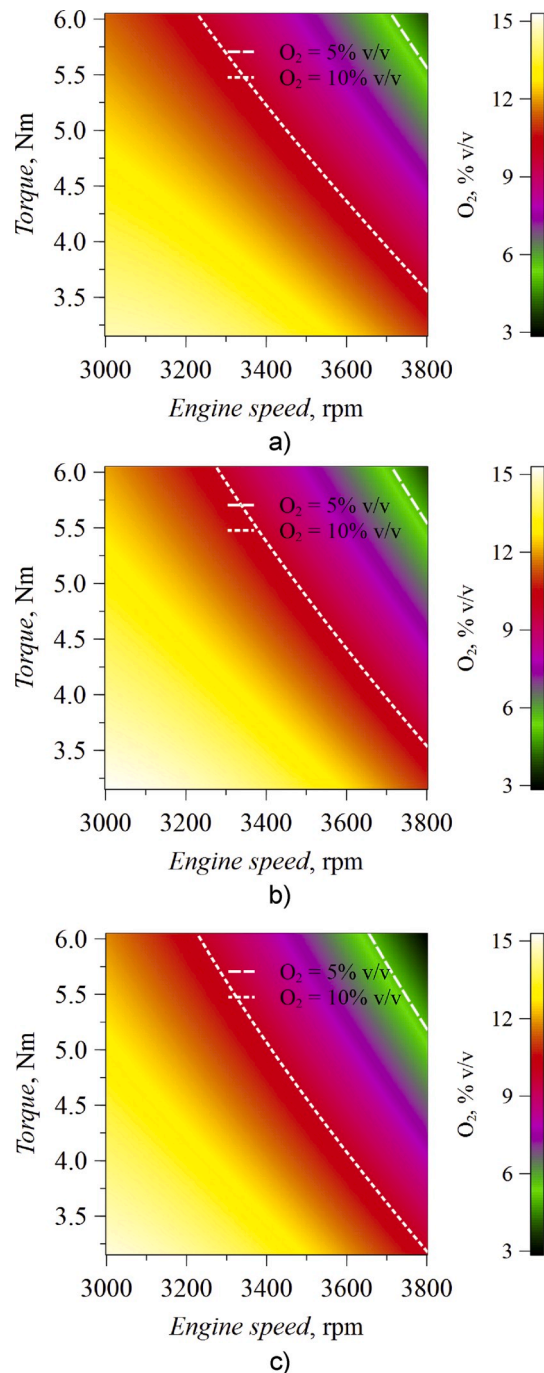
Fig. 5. Emission maps of O_2 for the operation with a) fossil diesel, b) 5% v/v biodiesel and 10% v/v biodiesel. Dashed and dotted lines represent isoconcentration contours.

with fossil diesel, there was a slight increase in O_2 emission for B5. On the other hand, O_2 emission for B10 resembles that of fossil diesel. It was found that for loads in the range of 5–95%, the effect of biodiesel content in the range B0–B100 on O_2 concentration was negligible [11]. A study with B100 found that, at constant engine speed, the equivalence ratio increases linearly with BMEP [24]. The O_2 emission maps obtained here are thus in agreement with those studies.
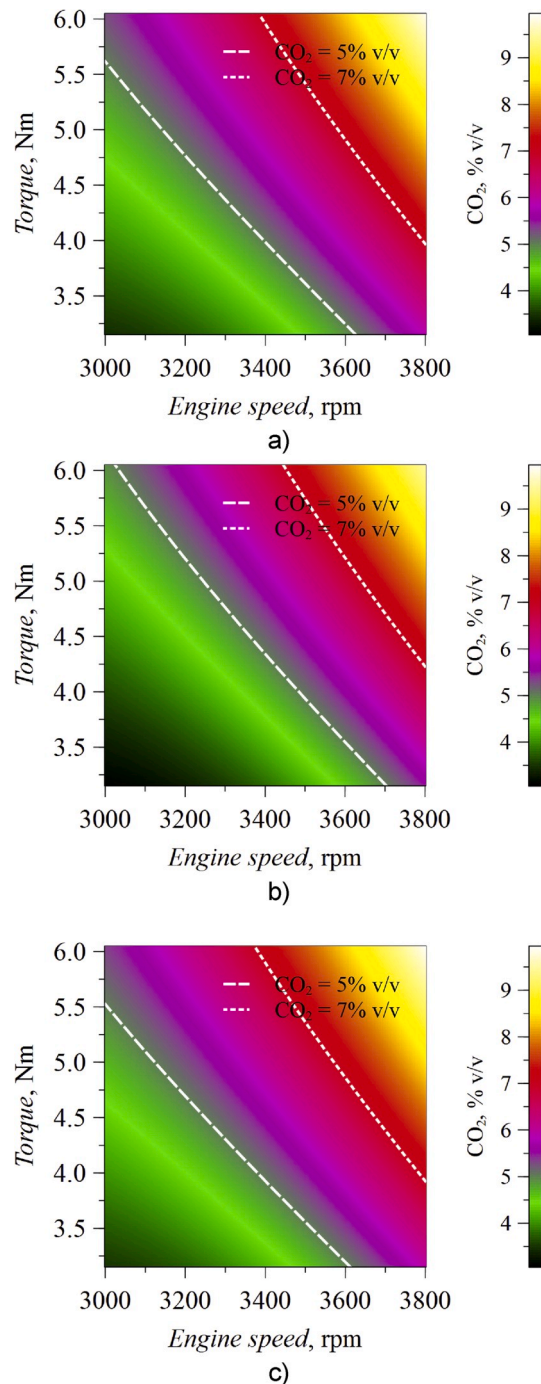
3.2.3. CO_2 emission map

Fig. 6a depicts the CO_2 emission map for the operation with fossil diesel. The CO_2 emission map features opposite trends when compared with the O_2 emission map. A direct proportion characterizes the dependence of CO_2 emission on both engine speed and

torque. When torque increases by 1.0 N m CO_2 concentration increases by 0.64% v/v at 3000 rpm and 2.2% v/v at 3800 rpm. When engine speed increases at constant torque, CO_2 emission increases linearly at first and then more rapidly. CO_2 is a primary combustion product, and its concentration depends on the fuel-to-air ratio, which increases with both engine speed and torque.

Studies with fossil diesel report a linear increase in CO_2 emission when engine load (or BMEP) increases at constant engine speed [11,24], which is consistent with our results. Under the same conditions, other studies found that CO_2 emission increases linearly at first and then more rapidly at the higher end of the studied load range [22,25]. The CO_2 emission profiles resulting from varying engine speed at full load shows maxima and minima [27] or a linear profile [26].

Fig. 6. Emission maps of CO_2 for the operation with a) fossil diesel, b) 5% v/v biodiesel and 10% v/v biodiesel. Dashed and dotted lines represent isoconcentration contours.

Fig. 6b and c shows the CO_2 emission map for the operation with B5 and B10. With respect to the operation with fossil diesel, there was a slight decrease in CO_2 emission for B5, but CO_2 concentrations for B10 show the same level. A study at constant engine speed using fossil diesel, diesel-biodiesel blends found that at low and medium loads, CO_2 emissions are rather similar [11]. Under the same conditions, another study reports CO_2 emissions slightly higher for B20 compared with fossil diesel [25]. Additionally, for all the blends, there was an increase in CO_2 emission at 80% and 95% load [11]. A slight increase in CO_2 emission with respect to fossil diesel was observed for B5 at full load and different engine speeds [26]. The difference between fossil diesel and B10 was more evident, and the CO_2 emission profile was no longer linear [26].
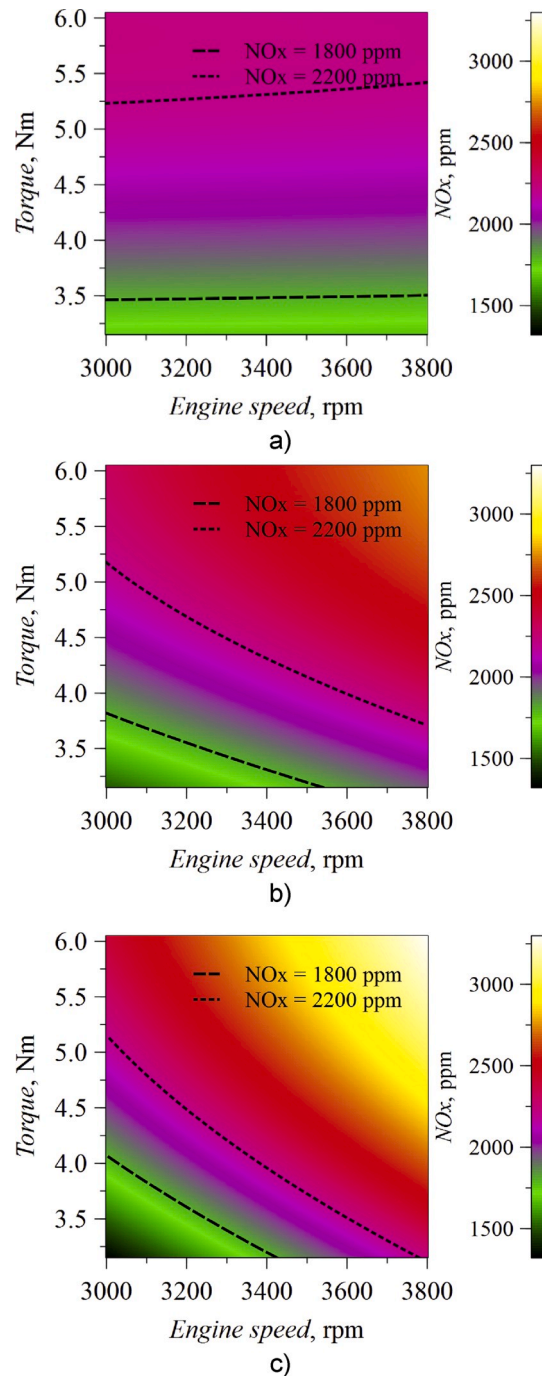
Fig. 7. Emission maps of NOx for the operation with a) fossil diesel, b) 5% v/v biodiesel and 10% v/v biodiesel. Dashed and dotted lines represent isoconcentration contours.

3.2.4. NOx emissions

NOx, composed of NO and NO_2, is a challenge for internal combustion engines [28]. Fig. 7a shows the NOx emission map for the operation with fossil diesel. A direct proportion characterizes the dependence of NOx emission on torque. Additionally, NOx emission is virtually independent of engine speed. At the lower end of the assessed torque range, NOx emission increases steadily but then slows down at the higher end. When engine speed increases at constant torque, NOx emission decreases slightly. Studies with fossil diesel report NOx emission profiles consistent with our result when the load (or BMEP) increases at constant engine speed [11,20]. Under the same conditions, another study reported an S-shaped NOx profile [25]. A plausible explanation for the latter is that the load range assessed here starts at the steadily growing section. In contrast to our findings, another study reports that NOx emission grows faster at the higher end of the load range [22].

Fig. 7b and c shows that the presence of biodiesel in the fuel significantly increases NOx emission, and several studies report this effect [11,25,26]. Within the assessed engine speed and torque ranges, NOx emission with B5 and B10 increases by 8.9% and 18%, respectively, with respect to fossil diesel. The reactions forming NOx are highly temperature-dependent [28], so higher operation temperatures characterize the operation with diesel-biodiesel fuel blends. In contrast to the operation with fossil diesel, B5 and B10 increase NOx emission linearly when engine speed increases at constant torque. Additionally, the presence of biodiesel in the fuel increases NOx emission beyond that of fossil diesel at the higher end of the assessed engine speed range while an opposite trend prevails at the lower end.

The dominant component of NOx is NO, with a reported share of 70–90% in compression ignition engines [28]. Thermal equilibrium calculations are the first approximation to NO and NO_2 emissions. Other predictive approaches are the Zeldovich, Fenimore, or fully detailed mechanisms. All these approaches present significant deviations of experiments [12], so direct measurements are a valuable tool for basic understanding and validations.

Fig. 8a and d shows the NO and NO_2 emission maps for the operation with fossil diesel. On average, NO accounts for 73% of the total NOx. Both NO and NO_2 emissions show similar profiles when torque increases at constant engine speed: steadily increasing at the lower end, slowing down at the higher end. On the other hand, NO and NO_2 emissions feature opposite linear trends when engine speed increases at constant torque: increasing for the former, decreasing for the latter. Fig. 8b and c illustrate the NO and Fig. 8e and f the NO_2 emission maps for the operation with B5 and B10, respectively. NO accounts for 76 and 80% of the total NOx for B5 and B10, respectively, which is within the reported range [28]. With biodiesel in the fuel, NO emission features similar profiles with torque (at constant engine speed) but reaches significantly lower levels at the lower end of the assessed engine speed range. Additionally, NO emission still increases linearly with engine speed (at constant torque), but at a significantly higher rate. On the other hand, NO_2 emission features similar profiles with torque (at constant engine speed), turns almost independent of engine speed for B5, and reaches lower levels at the lower end of the assessed engine speed range for B10. Finally, NO_2 emission shows a linear dependence on engine speed (at constant torque) but switches from a decreasing trend for fossil diesel to an almost constant value for B5 and an increasing trend for B10, as illustrated in Fig. 8d, e and 8f.

The regression models for CO, CO_2, and O_2 feature R^2 adjusted values greater than 0.8. The regression models for NO and NO_2 show a rather low R^2 adjusted value. A plausible explanation for the latter is that longer exposition times are required for those sensors. In any case, results were found to be qualitatively consistent with published literature. Both top-down and bottom-up selection procedures are recommended to fit the models and then select those with the highest R^2 value. Additional experiments can be done to further improve the models, especially those for NO and NO_2. Nevertheless, a successful methodology for constructing the models has been proved.

4. Conclusions

This work presents the development of CO, O_2, CO_2, NO, NO_2 and NOx emission maps for a diesel engine powered by diesel and diesel-biodiesel fuel blends. Experiments were carried out in a single-cylinder, four-stroke, air-cooled compression ignition engine covering nine experimental conditions corresponding to high, medium, and low torque and engine speed levels. The fuels were 100% diesel (B0), and blends with 5% (B5) and 10% (B10) biodiesel content. A successful methodology for constructing statistical models and then generate emission maps has been proved. Procedures such as engine calibration, aftertreatment optimization and emissions assessment in stationary operation can benefit from those emission maps.

The apparent discrepancies in CO emission trends among previous studies are explained based on the location of the studied engine speed and torque ranges with respect to a global minimum. The association between CO emission and fuel type was statistically non-significant. The lower end of the studied engine speed and torque ranges shows the highest O_2 emission and relatively high CO levels, which is consistent with a relatively low combustion temperature. Conversely, the upper end of the studied engine speed and torque ranges shows the lowest O_2 concentration due to the higher fuel-to-air ratio. With respect to B0, there is a slight increase in O_2 concentration for B5, but there are no noticeable differences with B10.

A direct proportion characterizes the dependence of CO_2 emission on both engine speed and torque. With respect to the operation with fossil diesel, there was a slight decrease in CO_2 emission for B5, but CO_2 emission for B10 rises again to the initial level. A direct proportion also characterizes the dependence of NOx emission on torque, although it is virtually independent of engine speed. Both NO and NO_2 emissions show similar profiles for B0 when torque increases at constant engine speed: steadily increasing at the lower end, slowing down at the higher end. On the other hand, NO and NO_2 emissions feature opposite linear trends when engine speed increases at constant torque: increasing for the former, decreasing for the latter. NOx emission for B5 and B10 increases by 8.9% and 18%, respectively, with respect to B0.
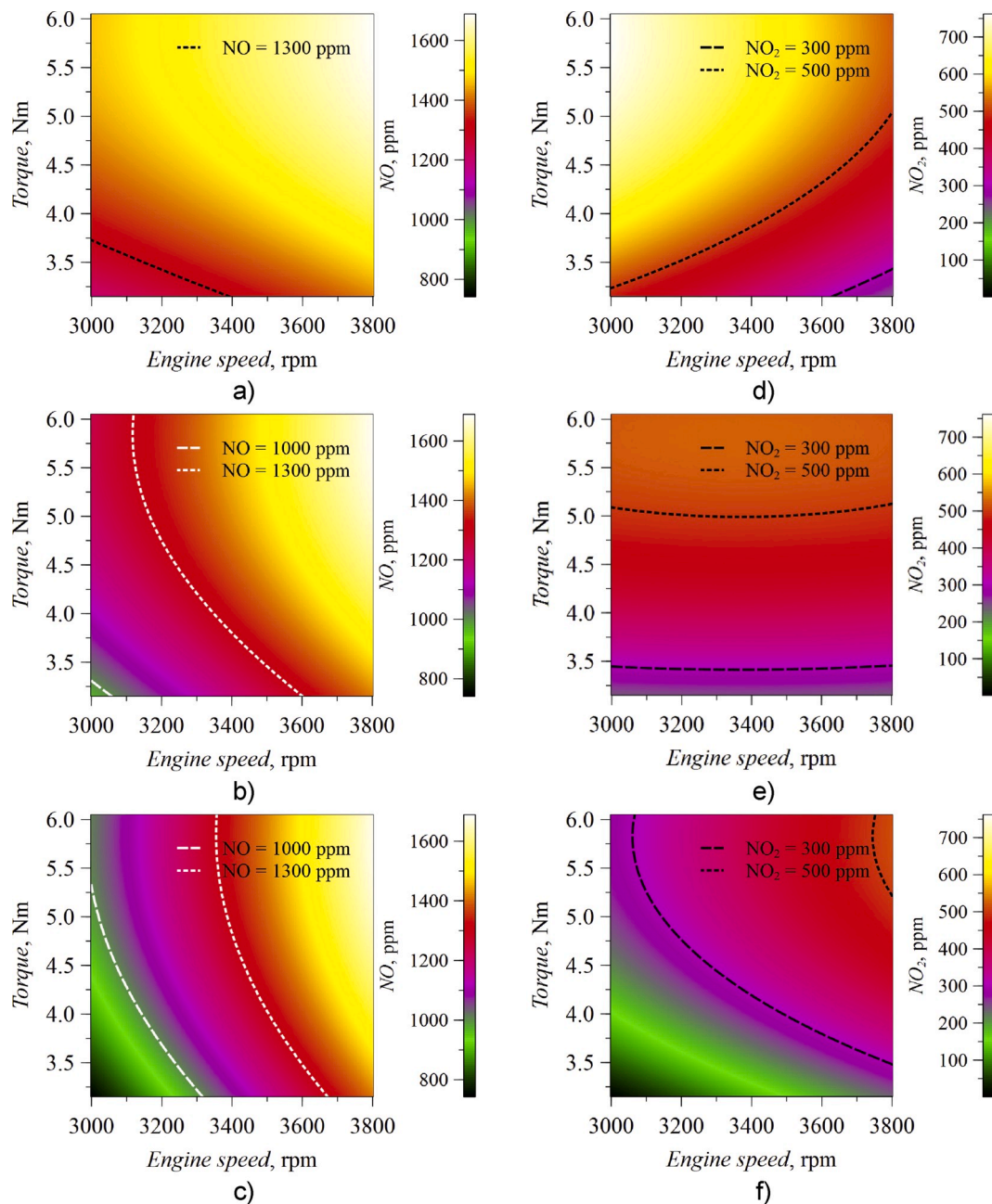
Fig. 8. Emission maps of NO and NO$_2$ for the operation with fossil diesel (a, d), 5% v/v biodiesel (b, e) and 10% v/v biodiesel (c, f). Dashed and dotted lines represent isoconcentration contours.

Declaration of competing interest

The authors declare that they have no known competing financial interests or personal relationships that could have appeared to influence the work reported in this paper.

CRediT authorship contribution statement

A. Mejía: Methodology, Software, Investigation. **M. Leiva:** Methodology, Software, Investigation. **A. Rincón-Montenegro:** Methodology, Software, Formal analysis, Writing - original draft. **A. Gonzalez-Quiroga:** Conceptualization, Validation, Writing - review & editing, Supervision. **J. Duarte-Forero:** Conceptualization, Validation, Formal analysis, Resources, Writing - original draft, Supervision.

Acknowledgments

References

[1] A.T. Hoang, Waste heat recovery from diesel engines based on Organic Rankine Cycle, Appl. Energy 231 (2018) 138–166, https://doi.org/10.1016/j.apenergy.2018.09.022.

[2] M. Tabatabaei, M. Aghbashlo, M. Dehhaghi, H.K.S. Panahi, A. Mollahosseini, M. Hosseini, M.M. Soufiyan, Reactor technologies for biodiesel production and processing: a review, Prog. Energy Combust. Sci. 74 (2019) 239–303, https://doi.org/10.1016/j.pecs.2019.06.001.

[3] C. Ericson, B. Westerberg, M. Andersson, R. Egnell, Modelling diesel engine combustion and NOx formation for model based control and simulation of engine and exhaust aftertreatment systems. https://doi.org/10.4271/2006-01-0687, 2006.

[4] X. Tauzia, A. Maiboom, H. Karaky, Semi-physical models to assess the influence of CI engine calibration parameters on NOx and soot emissions, Appl. Energy 208 (2017) 1505–1518, https://doi.org/10.1016/j.apenergy.2017.08.232.

[5] B. Rajesh Kumar, S. Saravanan, K. Rajaram, Combined effect of oxygenates and injection timing for low emissions and high performance in a diesel engine using multi-response optimisation, Alexandria Eng. J. 58 (2019) 625–636, https://doi.org/10.1016/j.aej.2019.03.009.

[6] B.P. BP, Energy outlook 2019 edition. https://www.bp.com/content/dam/bp/business-sites/en/global/corporate/pdfs/energy-economics/energy-outlook/bp-energy-outlook-2019.pdf, 2019.

[7] N.S. Ekaab, N.H. Hamza, M.T. Chaichan, Performance and emitted pollutants assessment of diesel engine fuelled with biokerosene, Case Stud. Therm. Eng. 13 (2019) 100381, https://doi.org/10.1016/j.csite.2018.100381.

[8] M.T. Chaichan, A.A.H. Kadhum, A.A. Al-Amiery, Novel technique for enhancement of diesel fuel: impact of aqueous alumina nano-fluid on engine's performance and emissions, Case Stud. Therm. Eng. 10 (2017) 611–620, https://doi.org/10.1016/j.csite.2017.11.006.

[9] A.K. Yadav, M.E. Khan, A.M. Dubey, A. Pal, Performance and emission characteristics of a transportation diesel engine operated with non-edible vegetable oils biodiesel, Case Stud. Therm. Eng. 8 (2016) 236–244, https://doi.org/10.1016/j.csite.2016.08.001.

[10] A.T. Hoang, V.V. Pham, A study of emission characteristic, deposits, and lubrication oil degradation of a diesel engine running on preheated vegetable oil and diesel oil, Energy Sources, Part A Recovery, Util. Environ. Eff. 41 (2019) 611–625.

[11] M.A. Ghadikolaei, L. Wei, C.S. Cheung, K.-F. Yung, Effects of engine load and biodiesel content on performance and regulated and unregulated emissions of a diesel engine using contour-plot map, Sci. Total Environ. 658 (2019) 1117–1130, https://doi.org/10.1016/j.scitotenv.2018.12.270.

[12] R. Rezaei, F. Dinkelacker, B. Tilch, T. Delebinski, M. Brauer, Phenomenological modeling of combustion and NOx emissions using detailed tabulated chemistry methods in diesel engines, Int. J. Engine Res. 17 (2015) 846–856, https://doi.org/10.1177/1468087415619302.

[13] J.A. Vélez Godiño, F.J. Jiménez-Espadafor Aguilar, M.T. García, Simulation of HCCI combustion in air-cooled off-road engines fuelled with diesel and biodiesel, J. Energy Inst. 91 (2018) 549–562, https://doi.org/10.1016/j.joei.2017.04.002.

[14] S. Roy, R. Banerjee, P.K. Bose, Performance and exhaust emissions prediction of a CRDI assisted single cylinder diesel engine coupled with EGR using artificial neural network, Appl. Energy 119 (2014) 330–340, https://doi.org/10.1016/j.apenergy.2014.01.044.

[15] K. Cheikh, A. Sary, L. Khaled, L. Abdelkrim, T. Mohand, Experimental assessment of performance and emissions maps for biodiesel fueled compression ignition engine, Appl. Energy 161 (2016) 320–329, https://doi.org/10.1016/j.apenergy.2015.10.042.

[16] S. Imran, D.R. Emberson, D.S. Wen, A. Diez, R.J. Crookes, T. Korakianitis, Performance and specific emissions contours of a diesel and RME fueled compression-ignition engine throughout its operating speed and power range, Appl. Energy 111 (2013) 771–777, https://doi.org/10.1016/j.apenergy.2013.04.040.

[17] H. Xu, B. Yin, S. Liu, H. Jia, Performance optimization of diesel engine fueled with diesel–jatropha curcas biodiesel blend using response surface methodology, J. Mech. Sci. Technol. 31 (2017) 4051–4059, https://doi.org/10.1007/s12206-017-0753-5.

[18] A.M. Taborda, R.A. Varella, T.L. Farias, G.O. Duarte, Evaluation of technological solutions for compliance of environmental legislation in light-duty passenger: a numerical and experimental approach, Transport. Res. Transport Environ. 70 (2019) 135–146, https://doi.org/10.1016/j.trd.2019.04.004.

[19] A.K. Yadav, A. Pal, A.M. Dubey, Experimental studies on utilization of prunus armeniaca L. (Wild apricot) biodiesel as an alternative fuel for CI engine, Waste and Biomass Valorization 9 (2018), https://doi.org/10.1007/s12649-017-9935-8, 1961–1969.

[20] V. Hariram, J.G. John, S. Seralathan, T. Micha Premkumar, Comparative analysis of combustion, performance and emission phenomenon of a CI engine fuelled with algal and cotton seed biodiesel, Int. J. Ambient Energy (2018) 1–12, https://doi.org/10.1080/01430750.2018.1562977.

[21] S. Sundaram, V. Ramasamy, N. Natarajan, J. Sivakumar, Investigation on performance and emission characteristics of cardanol–diesel blends in a single cylinder DI diesel engine, Energy Sources, Part A Recovery, Util. Environ. Eff. (2019) 1–11, https://doi.org/10.1080/15567036.2019.1587093.

[22] Y.D. Wang, T. Al-Shemmeri, P. Eames, J. McMullan, N. Hewitt, Y. Huang, S. Rezvani, An experimental investigation of the performance and gaseous exhaust emissions of a diesel engine using blends of a vegetable oil, Appl. Therm. Eng. 26 (2006) 1684–1691, https://doi.org/10.1016/j.applthermaleng.2005.11.013.

[23] L. Chen, S. Ding, H. Liu, Y. Lu, Y. Li, A.P. Roskilly, Comparative study of combustion and emissions of kerosene (RP-3), kerosene-pentanol blends and diesel in a compression ignition engine, Appl. Energy 203 (2017) 91–100, https://doi.org/10.1016/j.apenergy.2017.06.036.

[24] C.T. Chong, J.-H. Ng, S. Ahmad, S. Rajoo, Oxygenated palm biodiesel: ignition, combustion and emissions quantification in a light-duty diesel engine, Energy Convers. Manag. 101 (2015) 317–325, https://doi.org/10.1016/j.enconman.2015.05.058.

[25] S. Kumar, P. Dinesha, I. Bran, Influence of nanoparticles on the performance and emission characteristics of a biodiesel fuelled engine: an experimental analysis, Energy 140 (2017) 98–105, https://doi.org/10.1016/j.energy.2017.08.079.

[26] S.H. Hosseini, A. Taghizadeh-Alisaraei, B. Ghobadian, A. Abbaszadeh-Mayvan, Effect of added alumina as nano-catalyst to diesel-biodiesel blends on performance and emission characteristics of CI engine, Energy 124 (2017) 543–552, https://doi.org/10.1016/j.energy.2017.02.109.

[27] M.K. Yesilyurt, T. Eryilmaz, M. Arslan, A comparative analysis of the engine performance, exhaust emissions and combustion behaviors of a compression ignition engine fuelled with biodiesel/diesel/1-butanol (C4 alcohol) and biodiesel/diesel/n-pentanol (C5 alcohol) fuel blends, Energy 165 (2018) 1332–1351, https://doi.org/10.1016/j.energy.2018.10.100.

[28] C.R. Ferguson, A.T. Kirkpatrick, Internal Combustion Engines: Applied Thermosciences, third ed., John Wiley & Sons, 2016.